Research paper

# The urban heat island in Rio de Janeiro, Brazil, in the last 30 years using remote sensing data

Leonardo de Faria Peres[a,*], Andrews José de Lucena[b], Otto Corrêa Rotunno Filho[c],
José Ricardo de Almeida França[a]

[a] *Department of Meteorology, Federal University of Rio de Janeiro (UFRJ), Campus Ilha do Fundão—Cidade Universitária, 21949-900 Rio de Janeiro, RJ, Brazil*
[b] *Department of Geosciences, Agronomy Institute, Federal Rural University of Rio de Janeiro (UFRRJ), BR-465, Km 7, 23890-000 Seropédica, RJ, Brazil*
[c] *Civil Engineering Program, COPPE, Federal University of Rio de Janeiro (UFRJ), 21945-970 Rio de Janeiro, RJ, Brazil*

## ABSTRACT

The aim of this work is to study urban heat island (UHI) in Metropolitan Area of Rio de Janeiro (MARJ) based on the analysis of land-surface temperature (LST) and land-use patterns retrieved from Landsat-5/Thematic Mapper (TM), Landsat-7/Enhanced Thematic Mapper Plus (ETM+) and Landsat-8/Operational Land Imager (OLI) and Thermal Infrared Sensors (TIRS) data covering a 32-year period between 1984 and 2015. LST temporal evolution is assessed by comparing the average LST composites for 1984–1999 and 2000–2015 where the parametric Student *t*-test was conducted at 5% significance level to map the pixels where LST for the more recent period is statistically significantly greater than the previous one. The non-parametric Mann-Whitney-Wilcoxon rank sum test has also confirmed at the same 5% significance level that the more recent period (2000–2015) has higher LST values. UHI intensity between "urban" and "rural/urban low density" ("vegetation") areas for 1984–1999 and 2000–2015 was established and confirmed by both parametric and non-parametric tests at 1% significance level as 3.3 °C (5.1 °C) and 4.4 °C (7.1 °C), respectively. LST has statistically significantly (p-value < 0.01) increased over time in two of three land cover classes ("urban" and "urban low density"), respectively by 1.9 °C and 0.9 °C, except in "vegetation" class. A spatial analysis was also performed to identify the urban pixels within MARJ where UHI is more intense by subtracting the LST of these pixels from the LST mean value of "vegetation" land-use class.

## 1. Introduction

The 21 st century is the first "urban century", according to United Nations Development Programme. More than half the world's population (54%) currently lives in urban areas and projections made in 2014 (United Nations, 2014) suggest nearly two-thirds (one-third) will live in urban (rural) areas. In addition, United Nations (2014) predicts the number of megacities will increase from 28 in 2011–41 in 2030. In recent years much attention has been paid to the development of megacities due to its size and major problems they face, as well as almost all megacities are located in developing countries where urban growth rate is above the world average (United Nations, 2014). Accordingly, monitoring urban areas is important to understand its influence in different environmental parameters (Imhoff et al., 2010) and in weather and climate (Trenberth et al., 2007). In fact, urban construction materials have different thermal capacities and conductivities; the buildings geometry and their arrangements can trap radiation and

pollutants, and create a roughness surface influencing airflow and dispersion; engineering structures could remove surface water and change the natural drainage networks and the natural topography, hence changing the flow regimes and humidity. The net effect is a profound change in radiative, thermal, aerodynamic and moisture of the pre-existing surface features, resulting in changes in the natural balance of energy, mass, and momentum.

The urban heat island (UHI) formation, the most usual terminology for urban heating, is one of the most well-known forms of anthropogenic climate modification at the local level. It presents implications for human comfort and health, urban air pollution, energy management and urban planning. As pointed out by Imhoff et al. (2010), UHI phenomenon is associated with changes in surface, where drainage system quickly removes most of the rainwater on impervious materials. Accordingly, only a small portion of the net radiation is used for evaporation (latent heat flux) and most available radiation is used to warm land surface and air directly above (sensible heat flux). On the other

* Corresponding author at: Departamento de Meteorologia, Instituto de Geociências (IGEO), Universidade Federal do Rio de Janeiro, Av. Athos da Silveira Ramos, 274, CCMN (Bloco G), Campus Ilha do Fundão—Cidade Universitária, 21949-900 Rio de Janeiro, RJ, Brazil.
*E-mail address:* leonardo.peres@igeo.ufrj.br (L.d.F. Peres).

hand, a great fraction of the net radiation is used to evaporate water at moist surfaces in rural areas (e.g., lakes, rivers, soil, and vegetation) (Bretz et al., 1998; Taha, 1997; Arnfield, 2003). The thermal properties of the construction materials enable a faster heat transfer also contributing to increasing the temperature contrast between urban and non-urban areas. The spatial pattern contour of the isotherms forming one or several island features explains the UHI terminology. The isotherms distribution depends on the urban area configuration, but it is usually characterized by a strong thermal gradient in the urban-rural boundary, followed by a gradual rise in temperature toward the city core. The above description characterizes the classical UHI where the city center or downtown establish your core. However, several hot cores over the urban area may occur in large heterogeneous metropolitan areas forming a different pattern.

UHI phenomenon may be evaluated by comparing the air temperature in urban and rural environments based on automatic and conventional weather stations (e.g., Oke, 1976) and also by land-surface temperature (LST), usually obtained with thermal infrared (TIR) remote sensing data (Li et al., 2012; Chen and Yu, 2016). In situ air temperature data have the advantage of a high temporal resolution and historical time series, but have a low spatial resolution. On the other hand, remote sensing LST data have in general a low temporal resolution, but a high spatial distribution and is more easily related to surface conditions (Owen et al., 1998; Voogt and Oke, 2003; Imhoff et al., 2010). In fact, it is possible to retrieve biophysical land-surface characteristics and to describe urban environment materials based on remote sensing data. Consequently, remote sensing has potential to improve understanding the UHI phenomenon and its effects, and several studies have been assessed UHI using LST retrievals (e.g., Rao, 1972; Carlson et al., 1977; Matson et al., 1978; Gallo et al., 1995; Carnahan and Larson, 1990; Voogt and Oke, 2003; Weng and Quattrochi, 2006; Cheval et al., 2009; Li et al., 2011; Sobrino et al., 2012; Rhinane et al., 2012; Lucena et al., 2013).

Metropolitan area of Rio de Janeiro (MARJ) is currently going through a complex territorial transformation due to the construction of the Metropolitan Ring Road, Rio de Janeiro Petrochemical Complex (COMPERJ) and Itaguaí Port, one of the largest in the country. Metropolitan Ring Road will facilitate the production flow connecting different federal highways and expanding accessibility to Itaguaí Port and Rio de Janeiro city. Therefore it is expected that different companies are attracted to neighboring towns and along the Metropolitan Ring Road, which will connect the eastern and west end of MARJ.

In addition, the city of Rio de Janeiro and its metropolitan area are part of the megacities group. It is important that MARJ becomes part of a global research network investigating urban environment due to its worldwide exposure. This decade will be decisive for MARJ be promoted to the status of urban environmentally sustainable, starting with Rio + 20 UN Conference on Sustainable Development, which addressed the progress and setbacks of Rio 92, and the sporting events of the 2014 FIFA World Cup Brazil and Rio 2016 Summer Olympic Games, when both stimulate the promotion of sustainable practices and public policy strategies. Thus, it is important to monitor and create a database with information about the MARJ urban environment to collaborate for risk management of this area. In fact, UHI knowledge is fundamental to different areas of Earth sciences such as urban climatology, environmental changes, and human-environment interactions, and is important for planning and management practices. The interest of this work is to study surface UHI in MARJ using remote sensing data.

In this context, the objective of this paper is to 1) map LST between 1984 and 2015 in MARJ; 2) relate LST to land-use patterns; 3) determine the UHI magnitude, and 4) analyze MARJ thermal patterns.

## 2. Study area

MARJ is located in the southeastern Brazil and includes 21 cities (Fig. 1). Due to its geographical position and historical, economic and

political processes, MARJ is now the second pole of population concentration and economic activities of the country. The region has a large amount of sport and socio-cultural activities, specialized supply of goods and services, and a high level of urbanization.

The MARJ urban area pattern spreads from the central city region out in several directions over the metropolis. The total population during the twentieth century displays two well-defined trends: 1) a rise from the 1940s and 2) a stabilization in the 1990s, a pattern observed in the main Brazilian cities during these decades. Patterns of urban and rural population growth show an urban land-use consolidation related to the growth and decline in urban and rural population, respectively. In fact, urban population predominates since the 1940s, with over 1,000,000 people against 351,000 rural inhabitants. This fact reflects the population density growth in agreement with a marked human influence on the landscape. From the 1990s, the urban population has stabilized between 9 and 10 million.

The physical space is marked by distinct physiographic zones: lowlands, massif and hills, bays, ponds and lagoons and it suffers intense transformation, shaped by human social interactions. The lowlands and mountains represented a major challenge to urban growth. The social changes throughout history have resulted in a series of environmental system impacts on the MARJ physical space, such as dismantling hills, drainage of wetlands, rivers canalization, embankments, siltation and disposal of mangroves, lagoons, salt marshes and beaches (Lucena et al., 2013).

The peak precipitation and drought season over MARJ occur during Austral summer and winter, respectively, varying from 130 mm in January to 40 mm in July. Extratropical frontal systems, the South Atlantic Subtropical High (SASH), and the South Atlantic Convergence Zone (SACZ) influence the region as well as the MARJ topography. During Austral summer, extratropical frontal systems reaching MARJ interact with tropical convection resulting from humidity advection from the Amazon region. Extreme events of precipitation are related to SACZ intensification due to the convergence of the moisture from the Amazon region and the moisture transport from SASH (Kodama, 1992, 1993; Grimm, 2003; Coelho et al., 2016). Mean daily temperature vary from 26 °C (February) to 21 °C (July).

## 3. Method and data

In the following, we describe the data and methodology used to achieve the aims of this research as described in Section 1. A brief overview of the main steps for implementing the adopted methodology is given in the flowchart shown in Fig. 2.

The present study focusses on the analysis of a time series database composed by eighty-two images from Thematic Mapper (TM), Enhanced Thematic Mapper Plus (ETM + ) and Operational Land Imager (OLI) and Thermal Infrared Sensor (TIRS) onboard Landsat-5, 7 and 8 satellites covering a 32-year period between 1984 and 2015. We constructed this database by selecting images located in the path/row 217/76 (covering MARJ) with cloud coverage less than 10% and corresponding to the morning period (between 09 and 11 h).

Raw images were georeferenced using the polynomial model first degree and nearest neighbor interpolation in SPRING 4.3, a comprehensive GIS and Remote Sensing Image Processing software package developed by Brazilian National Institute for Spatial Research (INPE) (Camara et al., 1996). The Geocover_2003 dataset was the basis for georeferencing, which is a collection of standardized and orthorectified Landsat imagery (TM, and ETM + ) covering MARJ region. Both Landsat-5 TM (120 m) and Landsat-7 ETM + (60 m) band 6 images were resampled to 30 m spatial resolution according to the reflective spectral bands (Li et al., 2017). The Landsat Ground Processing System has resampled the Landsat-8 TIRS bands (100 m) by cubic convolution to 30 m and coregistered with the 30 m OLI spectral bands (Roy et al., 2014). We have separated the Landsat imagery database into two periods, i.e., 1984–1999 and 2000–2015 as shown in Table 1, to allow
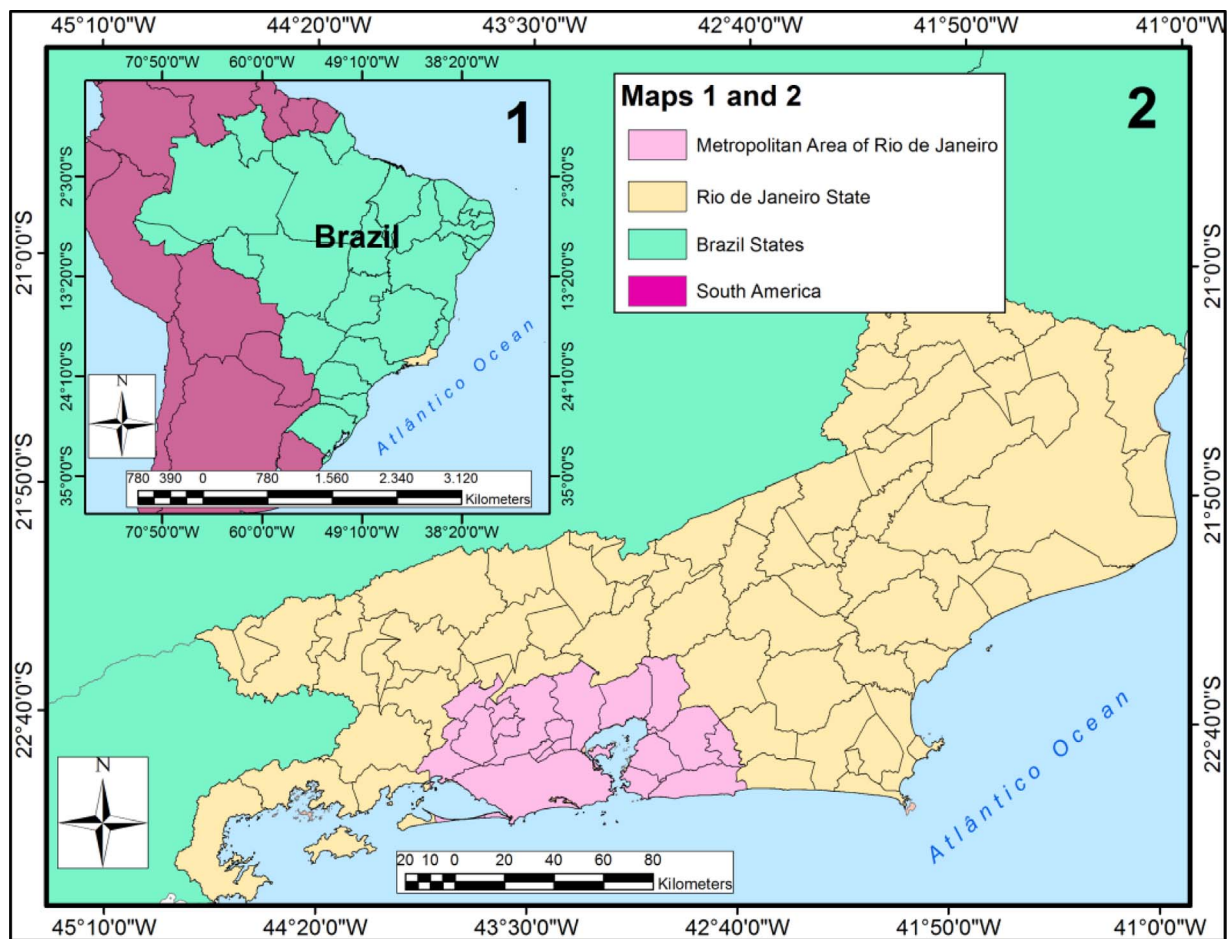
**Fig. 1.** Study Area.

observing the temporal evolution of UHI intensity.

Landsat calibration constants (Chander and Markham, 2003; Chander et al., 2009) were firstly used to convert raw data in digital numbers (DN) to radiance in all TM and ETM + (OLI and TIRS) bands. Hereafter the analogous OLI and TIRS bands are given in parentheses. The reflectance values in bands 1–5 (2–6) and 7 (7) were then computed based on the average solar irradiance in each band, the Earth–Sun distance, and the solar zenith angle. Radiance in band 6 (10) was converted into brightness temperature (BT) values based on the inversion of Planck function and Landsat-5 and 7 (8) calibration constants 1 and 2 (Qin et al., 2001).

In order to retrieve LST and to derive land-use maps from Landsat images, a simple cloud-masking algorithm was used to remove cloud-contaminated pixels, while maintaining cloud-free pixels as much as possible. The algorithm uses BT in band 6 (10) and reflectance values in bands 3 (4) and 4 (5) and is based on three techniques (Franca and Cracknell, 1995; Chen and Dudhia, 2001): 1) threshold value in band 3 (4), which for MARJ region it was selected as 0.3 after several tests; 2) threshold value for BT in band 6 (10) that was set as 278 K; and 3) the Q ratio method of band 4 (5) reflectance to band 3 (4) reflectance, which was close to unity for most cloudy pixels, less than 0.8 for most cloud-free water pixels, and greater than 1.6 for clear vegetation. However, as pointed out by Chen and Dudhia (2001) for barren soil in Texas, the Q ratio method has also failed in MARJ region to discriminate cloudy pixels from urban pixels as both samples have values between 0.8 and 1.6. Accordingly, we have followed Chen and Dudhia (2001) and adopted a supplementary test that takes into account BT in band 6 (10), where pixels were assumed as cloudy if the Q ratio fell between 0.8 and 1.6 and BT was less than 290 K.

LST retrieval is based on a single-channel algorithm (Qin et al., 2001; Jiménez-Muñoz and Sobrino, 2003; Souza and Silva, 2005) that uses a correction factor for BT in band 6 (10) taking into account both the atmospheric and emissivity influence in the signal recorded by the instrument onboard the satellite (Peres et al., 2014; Van de Griend and Owe, 1993). Although Landsat-8 TIRS bands 10 and 11 allows using split-window algorithms, the LST consistency over time was ensured by adopting the same single-channel algorithm used with TM and ETM + band 6. The LST algorithm assumes different generalizations and parameterizations in order to simplify the atmospheric correction by using solely meteorological data from regular weather station network, thus avoiding the use of atmospheric profiles and radiative transfer computations. Accordingly, air temperature at 2 m and relative humidity data were obtained from ten weather stations present in MARJ. Previous works have shown that such kind of approach provides LST error with RMSE ranging from 1.0 to 3.0 K depending on the water vapor content whereas single-channel algorithms based on the radiative transfer equation (RTE) provide better results with an global accuracy of 2.0 K (Qin et al., 2001; Barsi et al., 2005; Jiménez-Muñoz et al., 2009; Zhou et al., 2012; Vlassova et al., 2014; Windahl and de Beurs, 2016).

LST changes detection in tropical environments based on orbital remote sensing data largely depends on the number of available cloud-free images (Asner, 2001; Schroeder et al., 2008; Hilker et al., 2015). Landsat spatial resolution (30 m) ensures an adequate spatial analysis for UHI studies, but at the cost of a reduced number of images due to its temporal resolution (16 days). Analysis of the temporal evolution of UHI intensity from Landsat data should be performed by combining images over multiple years and therefore we have carried out a
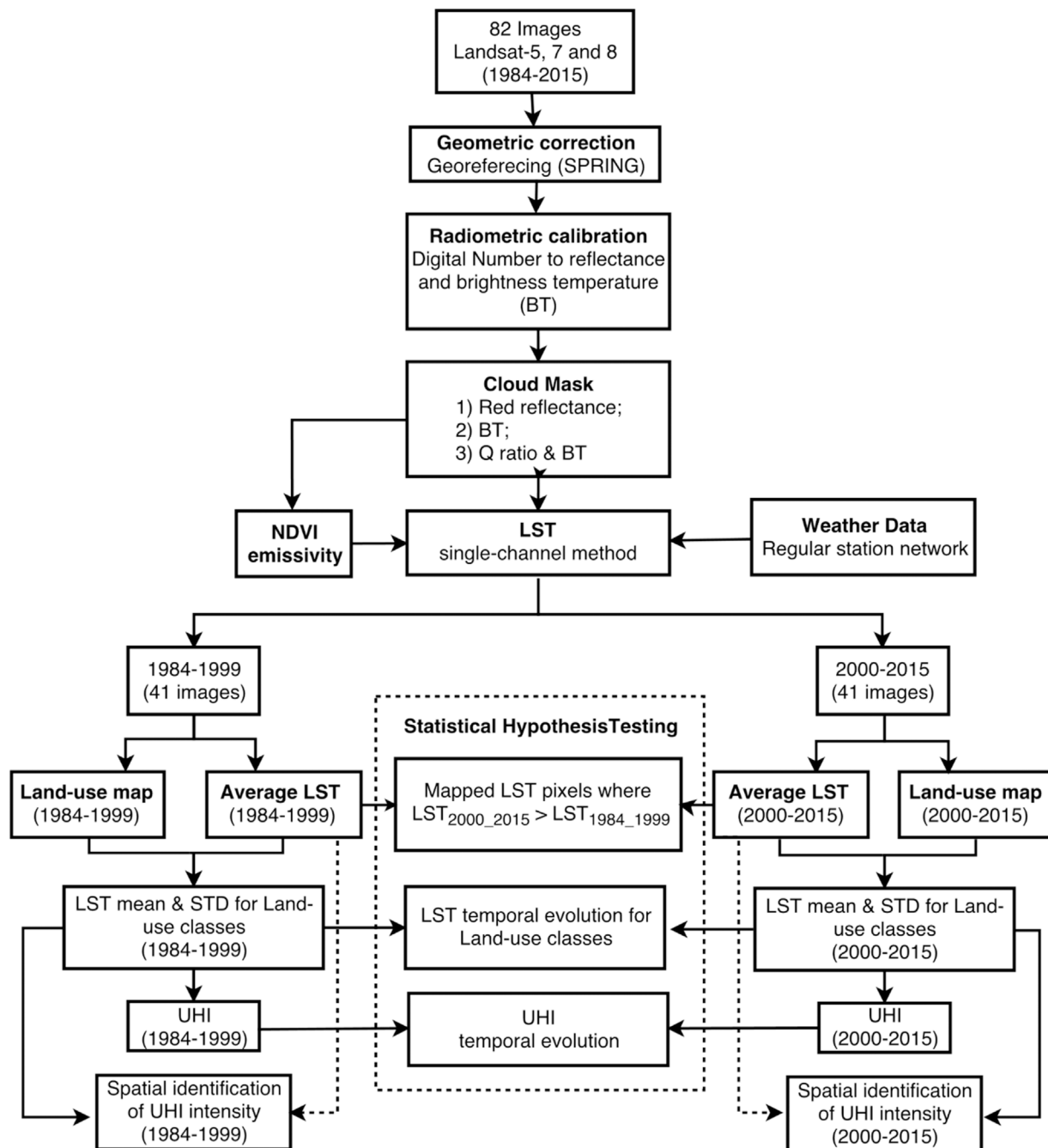
**Fig. 2.** Flowchart showing the data used and the main steps of the adopted methodology, where STD stands for standard deviation, Q is the ratio of near-infrared reflectance to read reflectance, and the statistical hypothesis tests are the *t*-test and the Wilcoxon-Mann-Whitney rank sum test.

sampling data design in order to obtain an appropriate relation between dataset aggregation and the resulting dataset size. The temporal sampling of Landsat images may properly represent the seasonality when they are aggregated into distinct seasons or quarterly periods, but the number of available clear sky observations acquired during a season is too low. On the other hand, Landsat images aggregation without separating them into distinct seasons makes the seasonality characterization more difficult, but the number of observations is higher. In this study, we divided the entire dataset, eighty-two images from 1984 to 2015, into two periods with the same amount of years (16) and images (41), but we have opted not to separate the images into distinct seasons, maintaining as many images as possible. In addition, each period has the same images per month in order to keep as much as possible the same seasonal distribution of Landsat images for each period ensuring

unbiased datasets and allowing the comparison between them. Fig. 3 shows the number of Landsat images available per month (the same for both periods) where the number of cloud-free images was lowest during November and highest in July. Finally, we have averaged multi-year LST observations retrieved for each period obtaining two average LST composites, respectively to the 1984–1999 and 2000–2015 periods.

An object-based supervised classification was used for creating land-use maps for the two above-mentioned periods, highlighting the land use and occupation in the MARJ. The image classification used was the Bhattacharya distance available in the SPRING 4.3 software package. Object-based classification approaches separate spatially and spectrally similar pixels as segmented objects. The classification starts with the segmentation that just splits the image into segmented objects that become the fundamental units of the image (Myint et al., 2011). This

**Table 1**
Landsat TM/ETM + /OLI & TIRS images used in this study. All images are located in the path/row 217/76. The superscript + (*) indicates Landsat-7 ETM + (Landsat-8 OLI & TIRS) images whereas those without indication refer to Landsat-5 TM. Landsat-5, 7 and 8 TIR bands have 120, 60, 100 m spatial resolution.

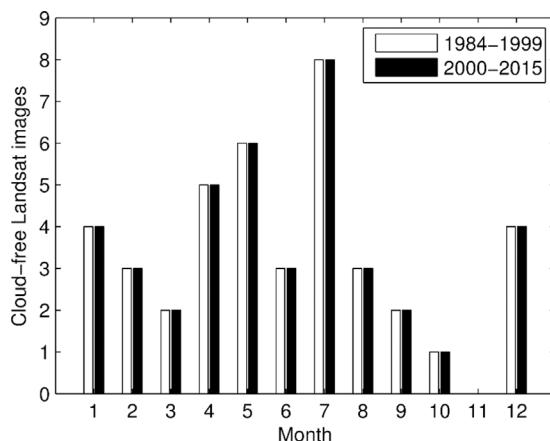| 1984–1999 | | 2000–2015 | |
| --- | --- | --- | --- |
| Date (YY/MM/DD) | Date (YY/MM/DD) | Date (YY/MM/DD) | Date (YY/MM/DD) |
| 1984/07/01 | 1993/04/05 | 2000/05/26 | 2010/07/09 |
| 1984/12/24 | 1994/01/18 | 2001/01/05 | 2011/05/09 |
| 1985/04/15 | 1994/05/10 | 2001/04/27 | 2011/07/12 |
| 1985/07/04 | 1994/07/29 | 2002/06/09[+] | 2011/09/30 |
| 1986/01/28 | 1994/10/01 | 2002/07/27[+] | 2013/04/28[*] |
| 1986/05/20 | 1995/04/11 | 2003/07/06 | 2013/05/14[*] |
| 1987/08/11 | 1995/04/27 | 2003/07/22 | 2013/07/17[*] |
| 1988/03/22 | 1995/05/29 | 2003/12/29 | 2013/08/02[*] |
| 1990/02/24 | 1995/07/16 | 2004/01/30 | 2014/01/09[*] |
| 1991/02/27 | 1996/05/31 | 2004/03/02 | 2014/06/02[*] |
| 1991/04/16 | 1996/07/02 | 2004/04/03 | 2014/07/04[*] |
| 1991/05/02 | 1996/09/20 | 2004/12/31 | 2014/08/21[*] |
| 1991/07/21 | 1996/12/09 | 2005/07/11 | 2014/12/27[*] |
| 1991/09/07 | 1997/06/03 | 2006/02/04 | 2015/01/12[*] |
| 1992/02/14 | 1998/06/06 | 2006/05/27 | 2015/02/13[*] |
| 1992/06/05 | 1998/07/08 | 2007/02/23 | 2015/05/20[*] |
| 1992/08/08 | 1998/08/25 | 2007/04/12 | 2015/06/05[*] |
| 1992/12/14 | 1999/03/21 | 2008/12/10 | 2015/08/08[*] |
| 1992/12/30 | 1999/05/24 | 2009/05/19 | 2015/09/25[*] |
| 1993/01/15 | 1999/07/27 | 2010/03/19 | 2015/10/11[*] |
| 1993/01/31 | | 2010/04/20 | |



**Fig. 3.** Number of cloud-free Landsat images available per month for 1984–1999 and 2000–2015 periods.

study used the edge-based segmentation technique for grouping areas with similar texture (Lucena et al., 2013). Conversely, to single pixels, the objects have spatial information and extra spectral information (e.g., mean and median).

Four land-use classes were pre-determined "urban", "rural or urban low density", "vegetation" and "water bodies", and then, we have defined 10 training samples representing each class in order to assign class values to segmented objects. The probability density function of each class is estimated based on the training samples and then the Bhattacharya distance between the classes is computed for each object. The output land-use map is reviewed and when necessary the classification is optimized based on auxiliary data. The accuracy assessment was performed by comparing the output land-use classification at a certain number of samples with a reference data. Following Congalton (1991), a minimum of 50 sample points for each land-use class was selected producing error matrices to evaluate the classification. Aerial photos and land-use maps for 1980, 1990 and 2000 from the Pereira Passos Institute (Institute for Urban Design – City Hall of Rio de

Janeiro) and Rio de Janeiro State Foundation Center for Statistics and Research (CPERJ) were used as the reference data. From the error matrix, the obtained Kappa index was around 0.73 for both land-use maps (Kazay et al., 2011). It is worth noting that the Bhattacharya classifier was compared with different methods (e.g., unsupervised k-means, supervised Euclidean distance and maximum likelihood), but it yielded the most accurate results.

We have assessed the LST temporal evolution for the entire study area by comparing the above-mentioned average LST composites. Simultaneously, the UHI intensity was defined by comparing the LST mean value of "urban" class ($\overline{LST_u}$) with the corresponding values of "vegetation" ($\overline{LST_v}$) and "rural or urban low density" ($\overline{LST_r}$) classes (Li et al., 2012). The hypothesis assumes that the "urban" class has the highest value of LST. Accordingly, two UHI intensity measures were defined as follows:

$$UHI_{(u-v)_i} = \overline{LST_{u_i}} - \overline{LST_{v_i}} \tag{1}$$

$$UHI_{(u-r)_i} = \overline{LST_{u_i}} - \overline{LST_{r_i}} \tag{2}$$

where $UHI_{(u-v)}$ is the UHI intensity between urban and vegetation areas, $UHI_{(u-r)}$ is the UHI intensity between urban and urban low density areas, and $i$ can be 1984–1999 and 2000–2015 periods. This procedure provides two UHI intensity values per period, respecting to 1984–1999 and 2000–2015. Thus, we have performed a LST comparison between classes per period as well as assessed the LST temporal evolution of each land cover class between periods. The comparison per period reveals the role of each land cover in LST, and the comparison between periods reveals the LST evolution in each class. Considering the MARJ topography (lowlands and mountains), the UHI intensity computation taken into account only pixels below 100 m.

A spatial analysis for each period was also performed to identify the urban pixels within MARJ where UHI is more intense by subtracting the LST of these pixels from the LST mean value of "vegetation" class ($\overline{LST_v}$) obtained in the former procedure.

It is worth noting, that all comparisons were verified by the parametric two-sample $t$-test for difference of means under one-tailed hypothesis test (Wilks, 2006). The test was applied to differences between means under independence, considering unequal variances in order to check whether two sample means calculated from the different database are statistically different. The non-parametric Wilcoxon-Mann-Whitney rank sum test was also used to test for the differences in location between the LST urban and vegetation samples. Accordingly, the aim is to test for a possible difference in location and the null hypothesis is that the two LST data batches have the same location. Based on these two statistical hypothesis tests, it was possible to evaluate three hypothesis a priori: 1) average LST for 2000–2015 is higher than the average for 1984–1999 partially due to urbanization increase; 2) the mean LST value for urban pixels ($\overline{LST_u}$) is higher than the average for vegetation pixels ($\overline{LST_v}$) resulting from the thermal properties of the different material that are composed of; and 3) considering the same land-use class, LST average may increase with time due to urban expansion.

## 4. Results

### 4.1. Land-Use mapping

The land-use in MARJ has a concentration of "urban" class in the eastern and western sector of Guanabara Bay and towards the west and south (Figs. 4 and 5). The western part of Guanabara Bay corresponds to the Guanabara Plain Land, which covers the entire north of the city of Rio de Janeiro and extends across southern fringe around the Tijuca Mountain. "Urban" class also moves northward through the cities of the Fluminense Plain Land. Another large urban area surrounds the eastern sector of the Guanabara Bay. "Urban" pixels are also identified in the far west and east, and around Pedra Branca and Mendanha Mountains.
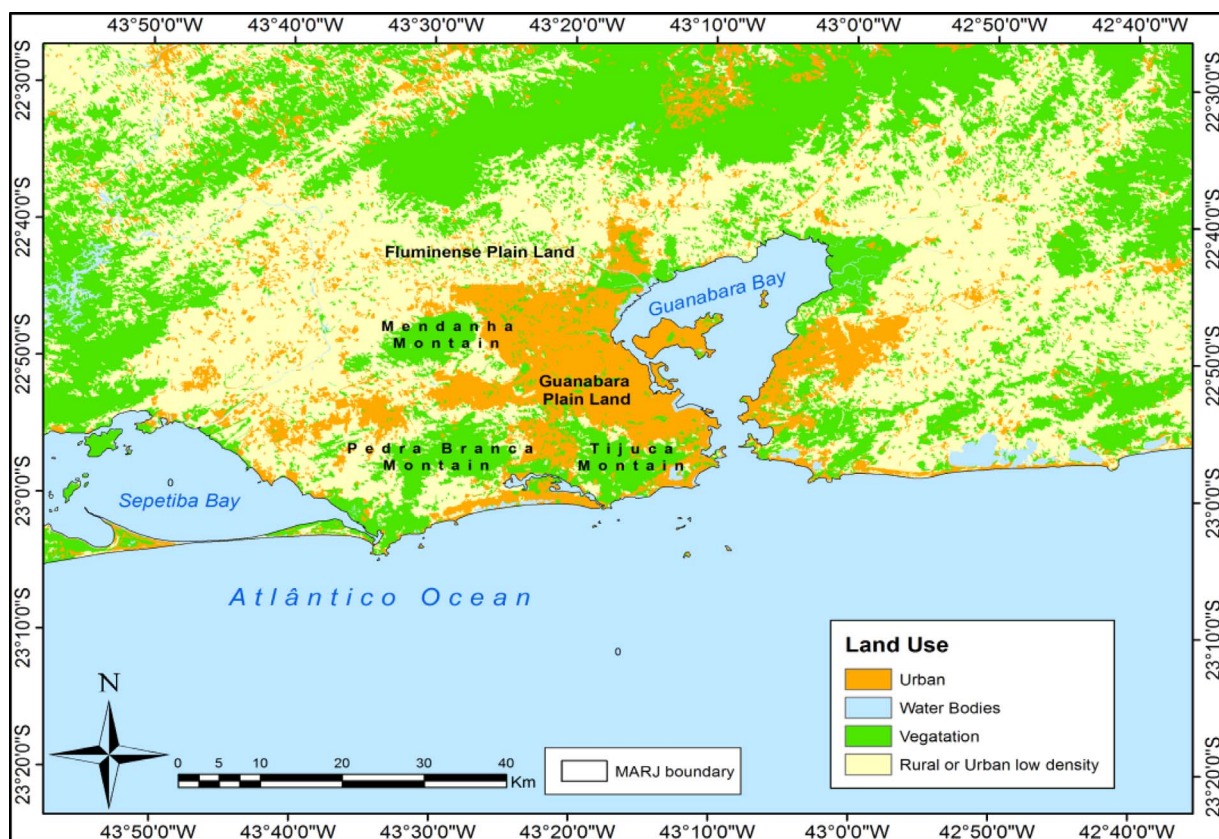
**Fig. 4.** Land use map for MARJ in the 1984–1999 period based on the object-based Bhattacharya supervised classification. Four land-use classes were pre-determined "urban", "rural or urban low density", "vegetation" and "water bodies".
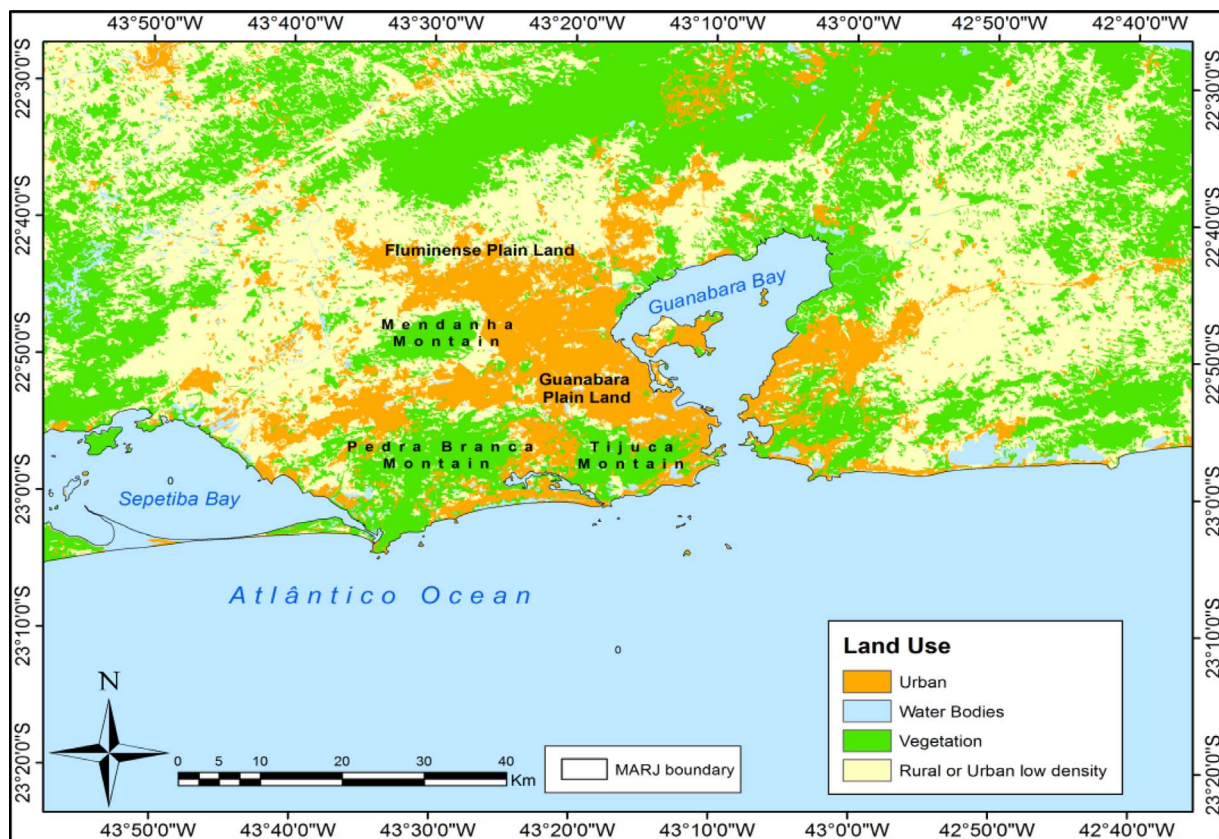


**Fig. 5.** Land use map for MARJ in the 2000–2015 period based on the object-based Bhattacharya supervised classification. Four land-use classes were pre-determined "urban", "rural or urban low density", "vegetation" and "water bodies".
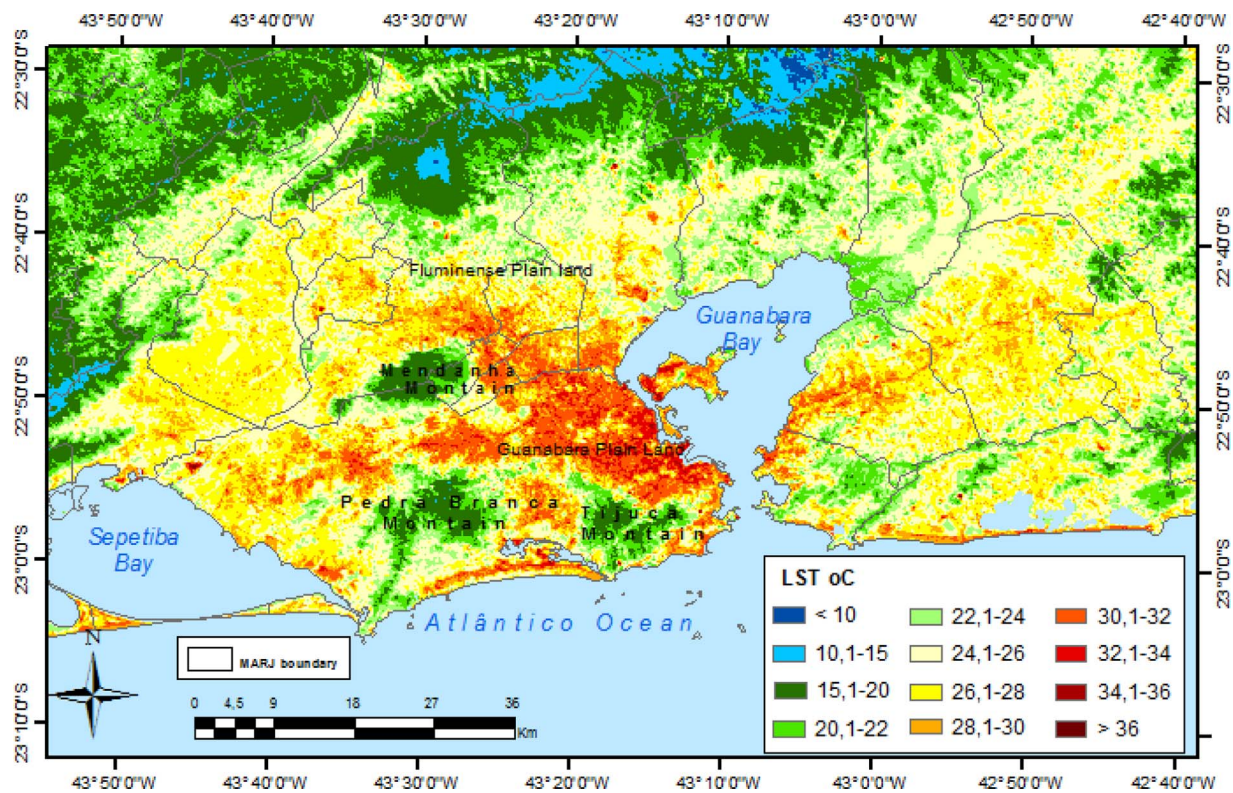
Fig. 6. Average LST composite for MARJ in the 1984–1999 period.

The "rural or urban low density" class predominates on the periphery of "urban" class (Figs. 4 and 5). The "vegetation" class is mainly concentrated in mountains (Tijuca, Pedra Branca, and Mendanha), at the foot of the Mar Mountain, until its higher altitudes, which starts from Sepetiba Bay, in the far west, and extends into the interior. "Vegetation" pixels may also be found at the swamp area located at the bottom of Guanabara Bay, and around coastal lagoons. Small mountains situated in the eastern region of the Guanabara Bay also show portions of vegetation.

The spatial pattern of the land-use follows the vectors of occupation and urban expansion in MARJ for these two periods. Evolution of land-use classes denotes a small increase in "urban", while "rural or urban low density" class presents the maximum increase. However, it is worth noting that this class is the more complex, which is defined during the segmentation process because of the metropolitan mixed-use.

### 4.2. Land-surface temperature

In the 1984–1999 period (Fig. 6), the highest LST values are located at lowlands areas around the mountains and along the coast, with values between 30 °C and 36 °C (red spots) coinciding with the "urban" class location. The hottest spot is concentrated in the western sector of Guanabara Bay toward the south, north, and west, and between Tijuca, Pedra Branca and Mendanha Mountains. In many of these places, the LST reaches extreme values, exceeding 36 °C, and in some areas above 40 °C. The eastern sector of the Guanabara Bay toward its end also presents values above 30 °C, but less intense. LST values below 30 °C (orange, yellow, green and blue colors) are restricted to "rural or urban low density" and "vegetation" classes. The lowest temperatures with LST values less than 20 °C occur in mountains.

In the 2000–2015 (Fig. 7), the hottest areas of the 1984–1999 period are maintained but the LST has increased reaching values above 36 °C. The warmer areas expand toward the extreme west, east and north. Industrial districts located in the far west presents the highest temperature with LST values around 43 °C. Areas with LST values

below 26 °C are restricted to western and eastern sectors.

As expected, maximum LST values were identified in "urban" land-use, while the minimum values were recorded in "vegetation" class for both 1984–1999 and 2000–2015 periods, revealing the role of land-use in LST values.

The Student t-test was applied to assess the LST temporal evolution for the entire study area by comparing the average LST composites between the two periods. The idea is to map within the significance level of 5% the pixels where LST for 2000–2015 is greater than the average for the 1984–1999 period. The results are shown in Fig. 8 where is depicted only the LST values considered statistically significant.

Fig. 8 shows the existence of different areas where LST for 2000–2015 is greater than the 1984–1990 period. There are significant pixels in the extremities north, west, and east of MARJ. The areas showing LST values above 30 °C are concentrated especially in major cities of Fluminense Plainland, as well as in cities located at eastern part of Guanabara Bay and in the neighborhoods of the west of Rio de Janeiro. Areas with averages between 26 °C and 30 °C (orange and yellow colors) are expressive in the east and west extreme of MARJ. LST values below 24 °C are also shown (green color) but lie beyond the limits of MARJ. It is worth noting that the observed areas showing significant pixels are coincident with those that have experienced great changes in the last 15 years, as the construction of COMPERJ, Itaguaí Port and the Metropolitan Ring Road at eastern, western and northern sectors of MARJ.

As an eventual unusual data (i.e., outliers) may invalidate the Student t-test, we have also used a resistant and robust nonparametric test, the so-called Mann-Whitney-Wilcoxon rank sum test (Wilks, 2006). This test is used to test for the differences in location between two data samples. Given the two 1984–1999 and 2000–2015 periods of independent LST data, the aim is to test for a possible difference in location. The null hypothesis is that the two LST samples have been drawn from the same period. The alternative hypothesis is that the center of the 2000–2015 period is expected in advance to be larger than
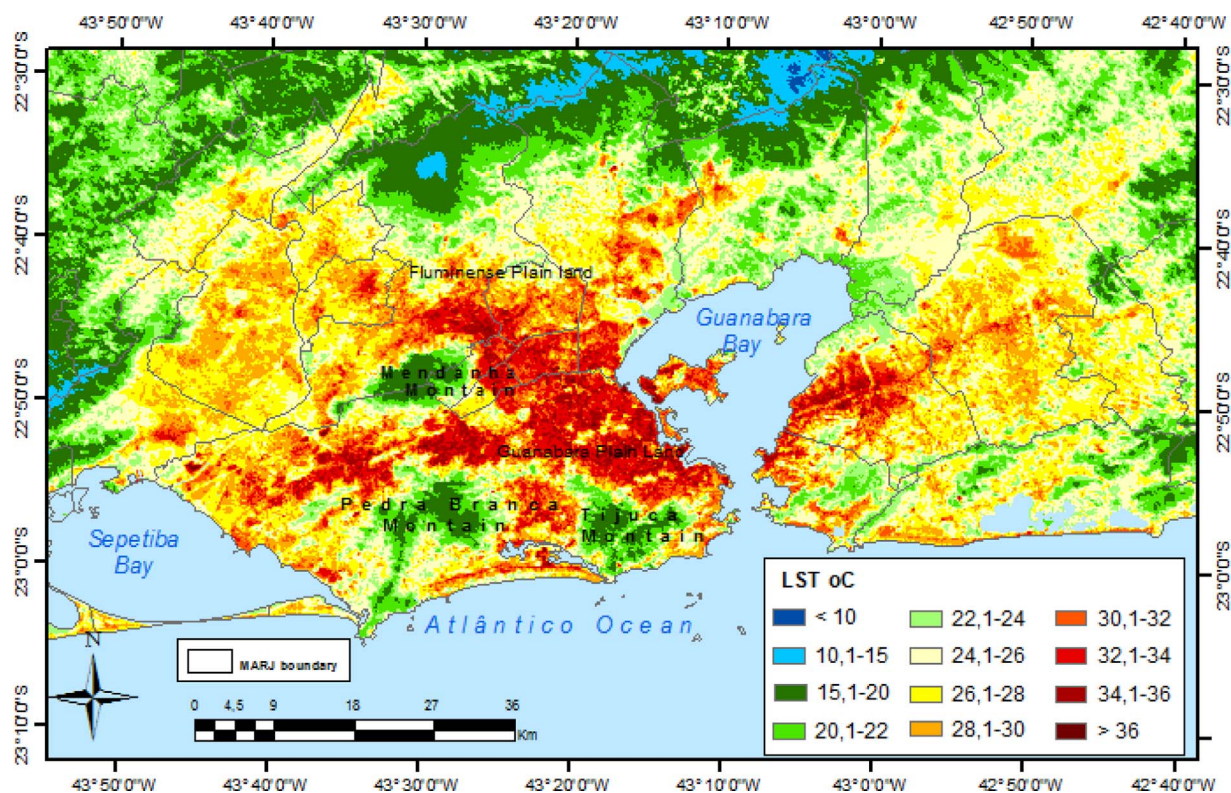
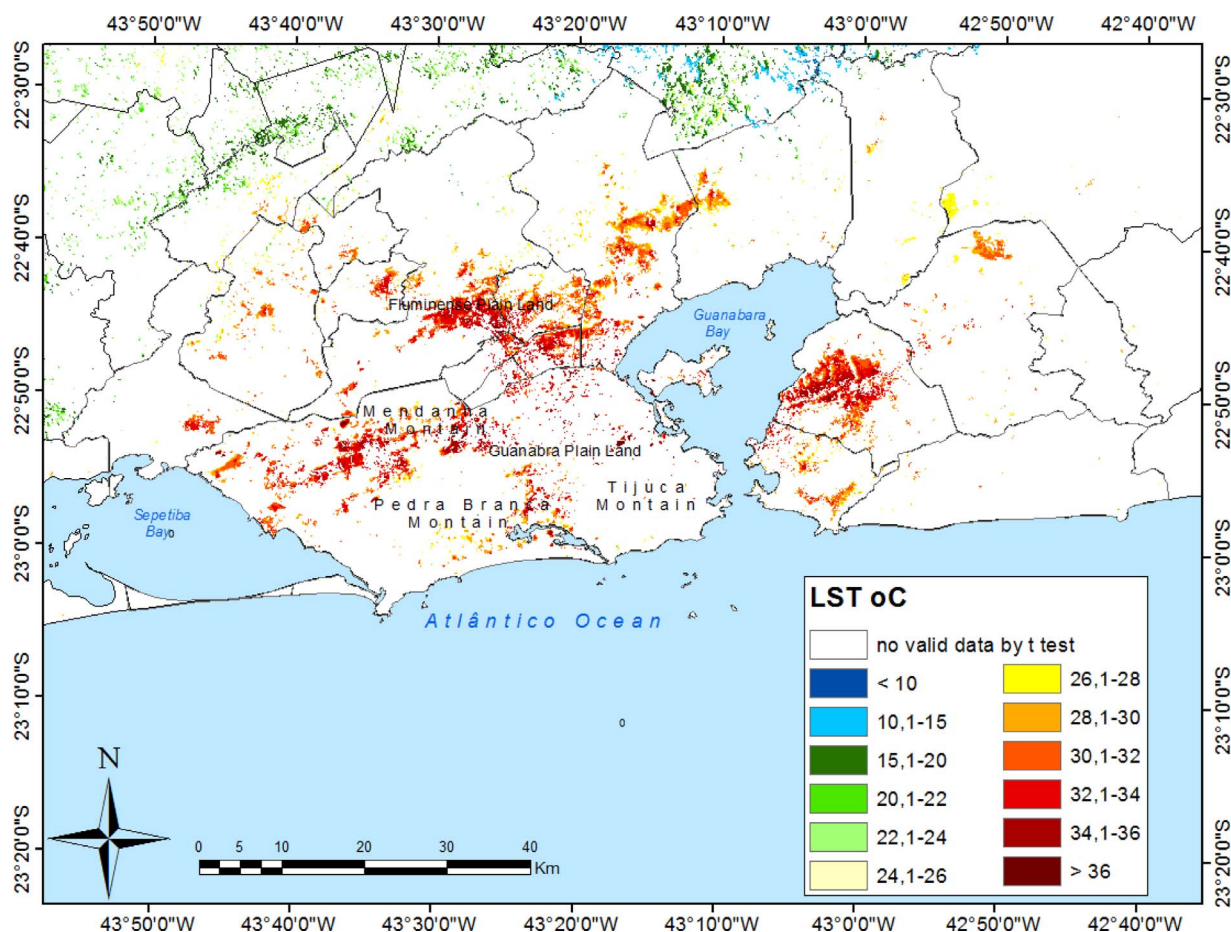**Fig. 7.** Average LST composite for MARJ in the 2000–2015 period.



**Fig. 8.** Areas where LST values for 2000–2015 is greater than the average for the 1984–1999 period according to the Student's *t*-test conducted at the 5% level.

**Table 2**

LST mean and standard deviation values for "urban", "vegetation" and "rural or urban low density" classes, and UHI intensity between urban and vegetation areas $UHI_{(u-v)}$ and between urban and urban low density areas $UHI_{(u-r)}$ in the 1984–1999 and 2000–2015 periods.

| Periods | Urban LST(°C) | | Vegetation LST(°C) | | Rural or urban low density LST(°C) | | Urban Heat Island (°C) | |
|---|---|---|---|---|---|---|---|---|
| | $\overline{LST_u}$ | $\sigma_{LST_u}$ | $\overline{LST_v}$ | $\sigma_{LST_v}$ | $\overline{LST_r}$ | $\sigma_{LST_r}$ | $UHI_{(u-v)}$ | $UHI_{(u-r)}$ |
| 1984–1999s | 28.8 | 2.3 | 23.5 | 2.4 | 25.5 | 1.6 | 5.1 | 3.3 |
| 2000–2015 | 30.7 | 2.6 | 23.7 | 2.1 | 26.3 | 1.9 | 7.1 | 4.4 |

the 1984–1999 period. LST data from the two periods that are being compared are pooled and ranked, consistent with the null hypothesis. LST observations are then segregated according to their labels of the 1984–1999 and 2000–2015 period, and the sums of the ranks of the two periods are computed. The null hypothesis can be rejected if the difference between the sums is sufficiently unusual. All tests performed to compare between periods based on the Mann-Whitney-Wilcoxon rank sum test resulted in the rejection of the null hypothesis at 5% significance level showing that the 2000–2015 period has higher LST values.

### 4.3. Land-use and urban heat island (UHI)

Table 2 shows the LST mean values ($\overline{LST}$) and the respective standard deviation ($\sigma_{LST}$) for "urban", "vegetation" and "rural or urban low density" classes for 1984–1999 and 2000–2015 periods, measuring the role of each land cover in LST and its evolution in each class. The UHI intensity is obtained for each period by computing the difference $\overline{LST_r}$ between $\overline{LST_u}$ and $\overline{LST_v}$, and between $\overline{LST_u}$ and

This procedure provides two UHI intensity values per period, and the UHI temporal variability. The power of the Student-t test and Mann-Whitney-Wilcoxon rank sum test depends on the sample size and the statistical significance obtained when comparing $\overline{LST_u}$, $\overline{LST_v}$, and $\overline{LST_r}$ are meaningless as the "urban", "vegetation" and "rural or urban low density" samples, from Landsat pixels, are very large (n > 10,000). With such kind of large sample, even very small differences between the LST mean values may be detectable. Accordingly, we randomly sampled 50 elements from the initial dataset in order to conduct these hypothesis tests for this subsample. It is worth noting that the mean and standard deviation for the subsample (not shown) are almost the same to those in Table 2 for the entire dataset.

Both parametric Student-t-test and non-parametric Mann-Whitney-Wilcoxon rank sum test have confirmed at 1% significance level that the mean LST for urban pixels is higher than the average LST for "vegetation" and "rural or urban low density" classes and the mean LST increased statistically significantly over time in all classes, except in "vegetation" class.

UHI intensity between urban and vegetation (urban and urban low density) areas for 1984–1999 and 2000–2015 periods was established as 5.1 °C (3.3 °C), and 7.1 °C (4.4 °C), respectively.

Results from Table 2 allow assessing the LST temporal evolution of each land cover class between 1984 and 1999 and 2000–2015 periods. It is worth noting that LST has increased statistically significantly (p-value < 0.01) over time in "urban" and "rural or urban low density" classes by 1.9 °C and 0.9 °C, respectively. In general, the pixels classified as "urban" and "rural or urban low density" are in fact a complex combination of different components as buildings, roads, grass, trees, soil, and water, which are less distinct in Landsat data because of its spatial resolution (30 m). The observed rise in "urban" and "rural or urban low density" LST can be related to the increase of those components associated with human activities and habitation leading to an increase in the impervious surface area within the pixel.

In addition, a simultaneous graphical comparison of LST values for each class is shown in Figs. 9 and 10 by using boxplots. These figures convey a large amount of information about the LST distribution for
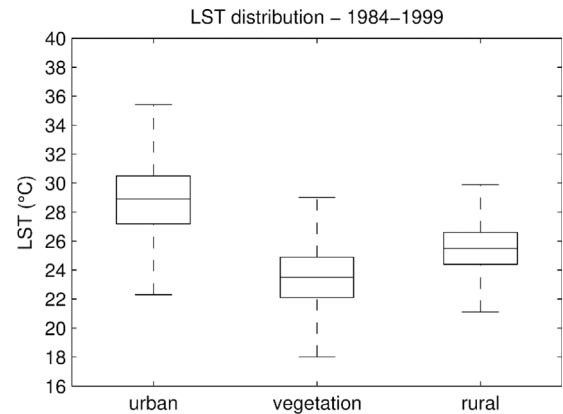
**Fig. 9.** Boxplot for the "urban", "vegetation" and "rural or urban low density" LST data respecting to the 1984–1999 period.
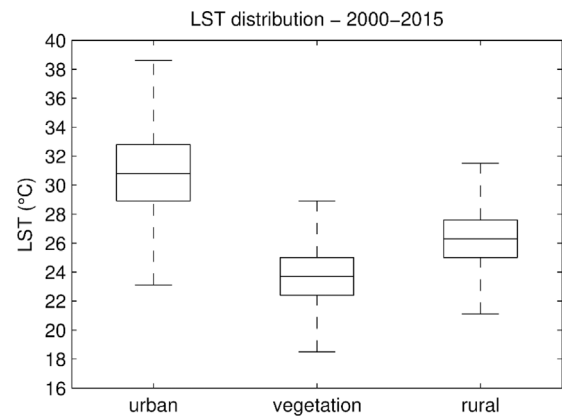
**Fig. 10.** Boxplot for the "urban", "vegetation" and "rural or urban low density" LST data respecting to the 2000–2015 period.

each class showing median (central mark), the lower and upper quartiles (edges of the box), the whiskers extend to the most extreme LST values the algorithm considers to be not outliers. The outliers are not plotted in the figures but considering that LST for each class is normally distributed the whiskers approximately cover 99.3% of LST data. It is worth noting that the mean is always very close to the median indicating that eventual outliers with very low or high LST values did not affect it. In general, the boxes occupy a small LST range showing that the data are concentrated quite near the median, which is more evident for the "rural or urban low density" class. These LST data are nearly symmetrical since the median is near the center and the whiskers are of comparable length. In agreement with the analysis based on the LST mean for each class (Table 2), "urban" and "vegetation" classes present the highest and lowest LST values, respectively, and it is observable that LST values for "urban" and "rural or urban low density" classes have increased over time. The urban LST values were more variable than the other classes and this fact is more evident in the 2000–2015 period.
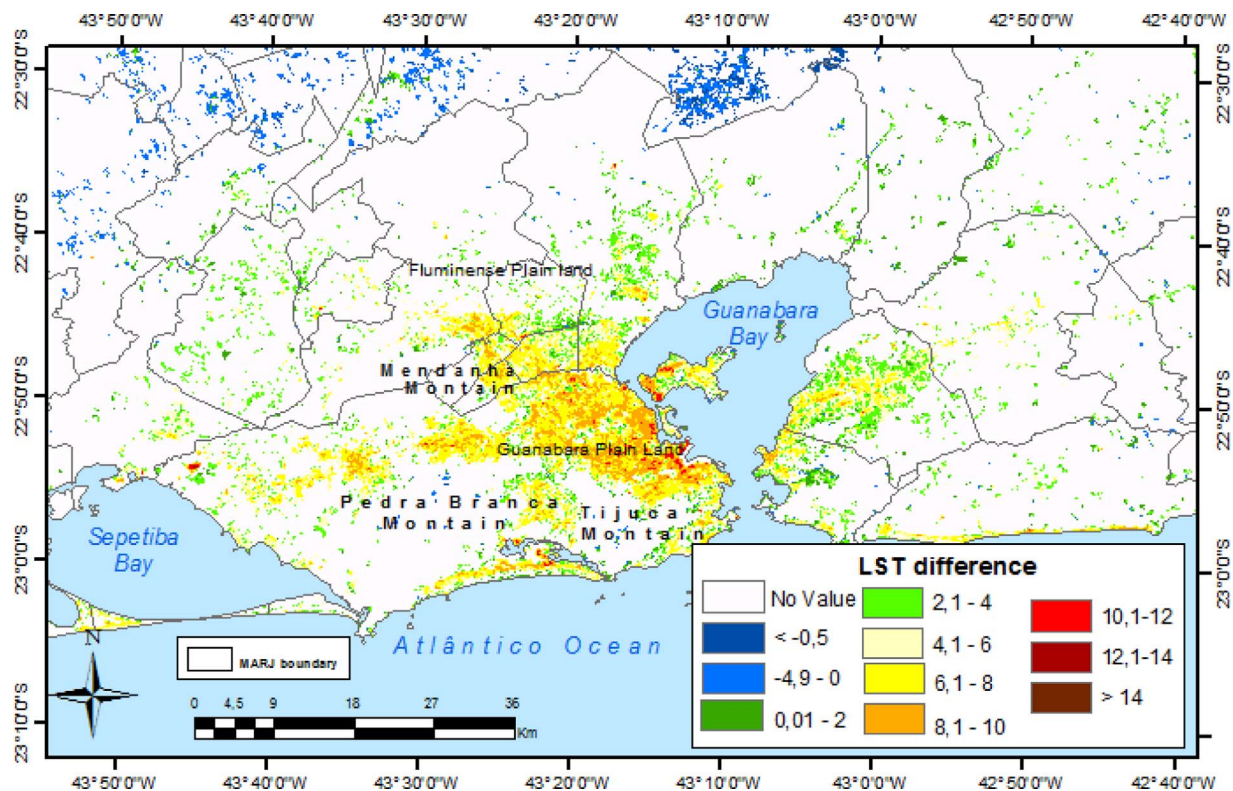
**Fig. 11.** Spatial identification of UHI intensity for the 1984–1999 period. LST difference is obtained by subtracting urban LST pixels from the LST mean value of "vegetation" class, which can be assessed in Table 2.

## 4.4. Spatial identification of UHI intensity

A spatial analysis was implemented to detect the urban pixels within MARJ where UHI is more intense by subtracting the LST of these pixels (i.e., only those classified as urban) from the LST mean value of "vegetation" class ($\overline{LST_v}$) obtained in the section 4.3 (see Table 2). The map for 1984–1999 period shows a spatial homogeneity, indicated by a large reddish spot (Fig. 11). It is apparent that the western edge of Guanabara Bay, the Downton and the Guanabara Lowland are the most heated areas and such locations are the oldest ones forming the metropolis and are considered as consolidated urban land. Accordingly, the thermal difference between vegetation is higher. Westerly, the reddish spot is more homogeneous in its first kilometers whereas in its final extension there are smaller differences with values less than 4 °C. This pattern reflects the western sector formation and expansion, which is still in the process of social and urban organization. Towards the eastern, western and northern end, the differences are smaller because of sparse urbanization and the presence of large areas with vegetation.

The spatial patterns of temperature gradients observed in 1984–1999 is preserved in the 2000–2015 period but expanded to other locations, where the far west, the south shore, the Guanabara lowland and the eastern sector of the Guanabara Bay are incorporated into a single unit thermal space reaching the highest LST values (Fig. 12). The great extent of this spot is explained by the "urban" growth in this area as discussed in section 4.1. A few areas located at eastern, western and northern end remain with weak thermal gradients, with differences below 6 °C. They are peri-urban areas that despite the urban sprawl, still retains rural features or native/semi-native vegetation. It is worth noting, an increase of cold spots (in green), with small differences between 2.1 and 4.0 °C, inside the most urbanized and the hottest MARJ area. These spots are associated with urban parks that reduce the temperature inside the urban space.

## 5. Conclusions

Approximately 30 years of Landsat-5, 7 and 8 data covering MARJ from 1984 to 2015 were used to compute mean LST composites for 1984–1999 and 2000–2015 periods in this work. Results based on both parametric Student-t-test and non-parametric Mann-Whitney-Wilcoxon rank sum test have shown the existence of different areas where LST for 2000–2015 is greater than 1984–1999, which may be used to indicate urban expansion.

The land use maps were essential to confirm the urbanization effect on LST. The joint analysis of the land-use maps and mean LST data for each period have shown that 1) regardless of the period, "urban" and "vegetation" classes always present the highest and lowest LST values, respectively. The LST of "rural or urban low density" is high, but always in between the "urban" and "vegetation" ones, representing a transition area involving rural and urban landscapes; and 2) regardless of the land-use class, LST has increased statistically significantly over time, except in "vegetation" class, with the highest rise in the "urban" (close to 2 °C) and lowest in the "rural or urban low density" classes (close to 1 °C). As expected, this study has confirmed that MARJ has physical and social characteristics favoring the UHI occurrence. Two UHI intensity measures were computed in this study, the first representing the LST difference between urban and vegetation areas and the second between urban and urban low-density areas. The former (latter) was established as 7.1 °C (4.4 °C) and 5.1 °C (3.3 °C) for 1984–1999 and 2000–2015 periods, respectively.

Previous studies have also focused on analyzing the UHI phenomenon in different cities around the world (e.g., Rome (Battista et al., 2016); Baghdad (Alobaydia et al., 2016); Posnán (Majkowska et al., 2017); Hong Kong (Paulinaa et al., 2015); Toronto (Wang et al., 2015); Guangzhou (Chen and Yu, 2016); Antofagasta, Lima, Guayaquil and Valparaiso (Palme et al., 2016)), but to the best of our knowledge, our work contributes to the existing literature by providing a useful methodology for combining a large number of images, covering the years
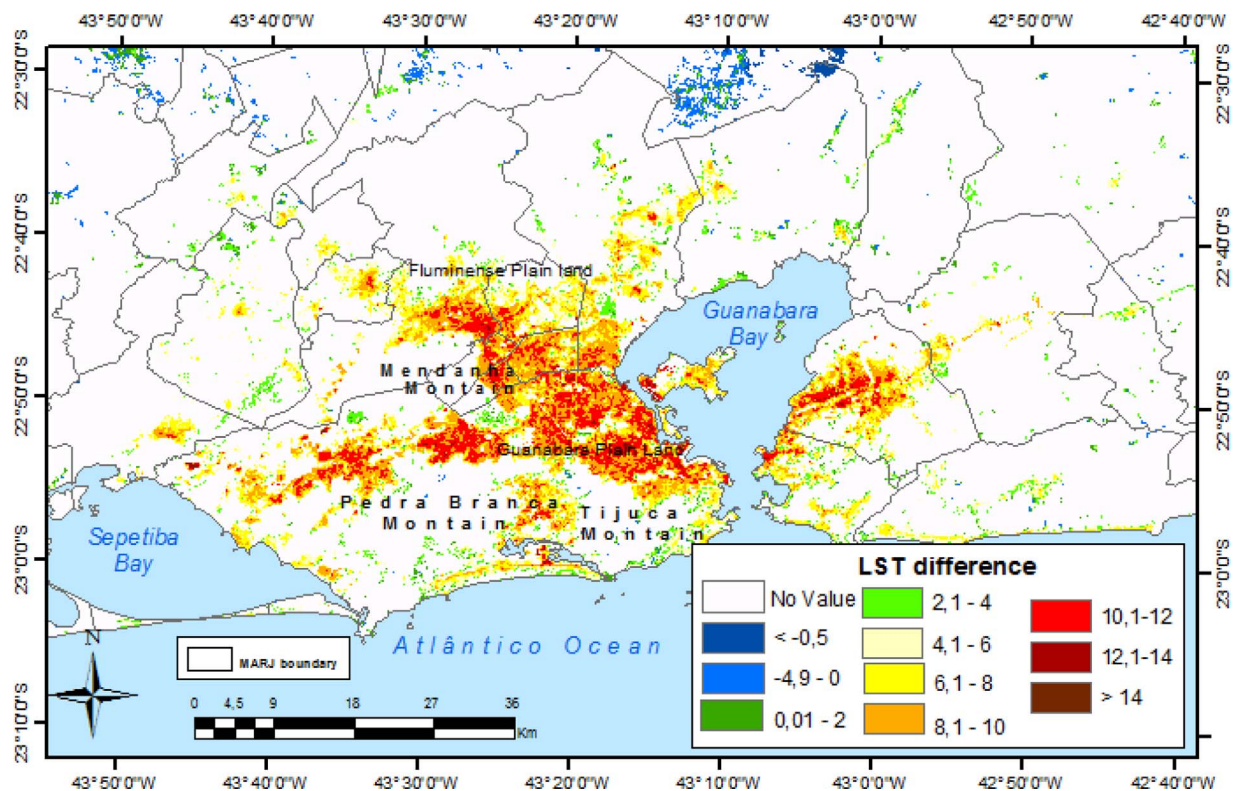
**Fig. 12.** Spatial identification of UHI intensity for the 2000–2015 period. LST difference is obtained by subtracting urban LST pixels from the LST mean value of "vegetation" class, which can be assessed in Table 2.

1984–2015, in order to assess the spatial and temporal patterns of UHI in MARJ. The methodology includes correcting atmospheric and emissivity effects for LST retrieval using Landsat TIR data and comparing the average LST composites for 1984–1999 and 2000–2015 using two statistical hypothesis tests (parametric and non-parametric) to map the pixels where LST for the more recent period is statistically significantly greater than the previous one.

In agreement with previous works (Li et al., 2012; Battista et al., 2016; Wang et al., 2015), our results show that the lowest LST values occur over vegetated areas. In fact, MARJ areas with relatively moderate temperature are located near the vegetated coastal massifs, coastal lagoons and in the northern region of the Guanabara Bay. Urban cool islands are also associated with urban parks and open landscapes. Such spaces within the complex urban system help to mitigate the UHI effect in MARJ. On the other hand, this work has shown heat spots with the same magnitude, but they are located in different urban areas within the metropolis in both the central area and suburbs or outskirts. In fact, the maximum UHI magnitude of 7.1 °C has not only occurred in the central business district of MARJ, which defines the classical UHI commonly observed in European and North Americans countries. Instead, MARJ seems a multinucleated metropolitan area presenting several hot cores distributed over its surface.

The UHI nomenclature used by Manley (1958) to describe the impacts of the urbanization on the city's atmosphere in London, England, assumes that the city develops and is organized in a space where the land-uses are very well-defined and identified. On the other hand, Roth (2007) has emphasized that urban climate studies in tropical countries may establish a distinctive view of the UHI configuration associated with temperate countries. In fact, urban or semi-urban areas in MARJ are mixed and vague, making it difficult to classify the land-uses. Such characteristics are typical of developing countries that carry particularities in the genesis, organization, and layout of cities. The suburbs of underdeveloped countries like Brazil show a very different role in the surface energy balance when compared to North American suburbs,

which are defined by Arnfield (2003) as comfortable places with well-spaced streets, green spaces, and public parks. The suburb of MARJ presents uncomfortable arid areas with little or no trees, poor housing and inadequate sanitation, which are heavily populated by people living in unsanitary conditions, such as slums. Thus, many suburban areas have recorded high-temperature values and in some cases even higher than the central area.

This study confirmed that LST changes detection based on TIR data depends on noise coming from undetectable clouds, cloud shadows, and aerosols, and on sample frequency that is largely reduced in a tropical environment because of clouds presence (Asner, 2001; Schroeder et al., 2008; Hilker et al., 2015). In fact, clouds increase the noise and decrease the number of available images. As LST is highly variable in space and time, estimates of noise based on high-frequency changes in LST over short periods is difficult. Spatial resolution/temporal resolution dichotomy is a constraint and must be taken into account in LST-based change detection studies on urban areas. Landsat TIR data allow a properly LST spatial analysis over urban areas but a poor sample frequency to characterize LST temporal variability, which can be further reduced by clouds. Landsat satellite series provide sufficient long-term records but show discontinuity in space and time due to clouds and orbits characteristics.

A constellation of satellites may overcome the problem by reducing the time gap between successive clear sky conditions (Pinheiro et al., 2008). LST can also be retrieved based on passive microwave measurements, but with a coarser spatial resolution and less accuracy because of the emissivity range in the microwave. On the other hand, microwave measurements are less sensitive to cloud contamination than TIR allowing LST retrieval in virtually all weather conditions (Pinheiro et al., 2008; Li et al., 2013). Clouds limit the space-time sampling of TIR LST measurements and the obtained LST dataset are biased as all observation refer to clear sky conditions. Hybrid methods taking advantages of TIR and microwave measurements is a promising topic for future studies trying retrieving LST with reasonable accuracy

and fine spatial resolution in cloudy conditions (Pinheiro et al., 2008; Li et al., 2013). Li et al. (2013) have indicated that further progress in LST retrieval can be achieved based on hyperspectral TIR sensors data and the exploration of the respective quantitative remote sensing techniques for LST and emissivity separation and atmospheric correction. In addition, future studies dealing with validation issues (more long-term sites and comparisons) and the angular dependence of LST is required to improve LST retrieval from orbital remote sensing data (Pinheiro et al., 2008; Li et al., 2013; Glob Temperatute Consortium, 2016).

## Acknowledgements

## References

Alobaydia, D., Bakarmana, M.A., Obeidata, B., 2016. The impact of urban form configuration on the urban heat island: the case study of baghdad. Iraq. Procedia Eng. 145, 820–827.

Arnfield, A.J., 2003. Two decades of urban climate research: a review of turbulence, exchanges of energy and water and the urban heat island. Int. J. Climatol. 23, 1–26.

Asner, G.P., 2001. Cloud cover in Landsat observations of the Brazilian Amazon. Int. J. Remote Sens. 18, 3855–3862.

Barsi, J.A., Schott, J.R., Palluconi, F.D., Hook, S.J., 2005. Validation of a Web-based Atmospheric Correction Tool for Single Thermal Band Instruments. pp. 58820E–58820E-58827.

Battista, G., Carnielo, E., Vollaro, R.D.-L., 2016. Thermal impact of a redeveloped area on localized urban microclimate: a case study in Rome. Energy Build. 133, 446–454.

Bretz, S., Akbari, H., Rosenfeld, A., 1998. Practical issues for using solar-reflective materials to mitigate urban heat islands. Atmos. Environ. 32, 95–101.

Camara, G., Souza, R.C.M., Freitas, U.M., Garrido, J., 1996. SPRING: Integrating remote sensing and GIS by object-oriented data modelling. J. Comput. Graph. 20, 395–403.

Carlson, T.N., Augustine, J.N., Boland, F.E., 1977. Potential application of satellite temperature measurements in the analysis of land use over urban areas. Bull. Am. Meteorol. Soc. 58, 1301–1303.

Carnahan, W.H., Larson, R.C., 1990. An analysis of an urban heat sink. Remote Sens. Environ. 33, 65–71.

Chander, G., Markham, B.L., 2003. Revised Landsat-5 TM radiometric calibration procedures, and post-calibration dynamic ranges. IEEE Trans. Geosci. Remote Sens. 41, 2674–2677.

Chander, G., Markham, B.L., Helder, D.L., 2009. Summary of current radiometric calibration coefficients for Landsat MSS, TM, ETM+, and EO-1 ALI sensors. Remote Sens. Environ. 113, 893–903.

Chen, F., Dudhia, J., 2001. Coupling an advanced land-surface/hydrology model with the Penn State/NCAR MM5 modeling system. Part II: preliminary model validation. Mon. Weather Rev. 129, 587–604.

Chen, Y., Yu, S., 2016. Impacts of urban landscape patterns on urban thermal variations in Guangzhou, China. Int. J. Appl. Earth Obs. Geoinf. 54, 65–71.

Cheval, S., Dumitrescu, A., Bell, A., 2009. The urban heat island of Bucharest during the extreme high temperatures of July 2007. Theor. Appl. Climatol. 97, 391–401.

Coelho, C.A.S., de Oliveira, C.P., Ambrizzi, T., et al., 2016. The 2014 southeast Brazil austral summer drought: regional scale mechanisms and teleconnections. Clim. Dyn. 46, 3737–3752.

Congalton, R.G., 1991. A review of assessing the accuracy of classifications of remotely sensed data. Remote Sens. Environ. 37, 35–46.

Franca, G.B., Cracknell, A.P., 1995. A simple cloud masking approach using NOAA AVHRR daytime data for tropical areas. Int. J. Remote Sens. 16, 1697–1705.

Gallo, K.P., Tarpley, J.D., Mcnab, A.L., et al., 1995. Assessment of urban heat islands: a satellite perspective. Atmos. Res. 37, 37–43.

GlobTemperatute Consortium, 2016. Annual User Assessment Report. Organisation: Consortium GlobTemperature, pp. 1–68 (Ref.: GlobT-WP23-DEL-21).

Grimm, A.M., 2003. The El Niño impact on summer monsoon in Brazil: regional processes versus remote influences. J. Clim. 16, 263–280.

Hilker, T., Lyapustin, A.I., Hall, F.G., Myneni, R., Knyazikhin, Y., Wang, Y., Tucker, C.J., Sellers, P.J., 2015. On the measurability of change in Amazon vegetation from MODIS. Remote Sens. Environ. 166, 233–242.

Imhoff, M.L., Zhang, P., Wolfe, R.E., Bounoua, L., 2010. Remote sensing of the urban heat island effect across biomes in the continental USA. Remote Sens. Environ. 114, 504–513.

Jiménez-Muñoz, J.C., Sobrino, J.A., 2003. A generalized single channel method for retrieving land surface temperature from remote sensing data. J. Geophys. Res. 108, 2–9.

Jiménez-Muñoz, J.C., Cristobal, J., Sobrino, J.A., Soria, G., Ninyerola, M., Pons, X., 2009. Revision of the single-Channel algorithm for land surface temperature retrieval from landsat thermal-infrared data. Geosci. Remote Sens. IEEE Trans. 47, 339–349.

Kazay, D.F., Lucena, A.J., Rotunno Fiçho, O.C., Peres, L.F., França, J.R.A., 2011. Mudança no uso e cobertura do solo e sua influência na temperatura de superfície: um estudo

na Região Metropolitana do Rio de Janeiro. XV Simpósio Brasileiro De Sensoriamento Remoto 752–759 (in Portuguese).

Kodama, Y.M., 1992. Large-scale common features of sub-tropical precipitation zones (the Baiu Frontal Zone, the SPCZ, and the SACZ). Part I: characteristics of subtropical frontal zones. J. Meteorolog. Soc. Jpn. 70, 813–835.

Kodama, Y.M., 1993. Large-scale common features of sub-tropical precipitation zones (the Baiu Frontal Zone, the SPCZ, and the SACZ). Part II: conditions of the circulations for generating the STCZs. J. Meteorolog. Soc. Jpn. 71, 581–610.

Li, J., Song, C., Cao, L., Zhu, F., Meng, X., Wu, J., 2011. Impacts of landscape structure on surface urban heat islands: a case study of Shanghai, China. Remote Sens. Environ. 115, 3249–3263.

Li, Y., Zhang, H., Kainz, W., 2012. Monitoring patterns of urban heat islands of the fast-growing Shanghai metropolis, China: using time-series of LandsatTM/ETM+ data. Int. J. Appl. Earth Obs. Geoinf. 19, 127–138.

Li, Z., Tang, B., Wu, H., Ren, H., Yan, G., Wan, Z., Trigo, I.F., Sobrino, J.A., 2013. Satellite-derived land surface temperature: current status and perspectives. Remote Sens. Environ. 131, 14–37.

Li, Z., Zhang, H.K., Roy, D.P., Yan, L., Huang, H., Li, J., 2017. Landsat 15-m panchromatic-assisted downscaling (LPAD) of the 30-m reflective wavelength bands to sentinel-2 20-m resolution. Remote Sens. 9 (755), 1–18.

Lucena, A.J., Rotunno Filho, O.C., França, J.R.A., Peres, L.F., Xavier, L.N.R., 2013. Urban climate and clues of heat island events in the metropolitan area of Rio de Janeiro. Theor. Appl. Climatol. 111, 497–511.

Majkowska, M., Kolendowicz, L., Półrolniczak, M., Hauke, J., Czernecki, B., 2017. The urban heat island in the city of Poznań as derived from Landsat 5 TM. Theor. Appl. Climatol. 128, 769–783.

Manley, G., 1958. On the frequency of snowfall in metropolitan England. Quart. J. R. Meteorol. Soc. 84, 70–72.

Matson, M., Mcclain, E.P., Mcginnis Jr., D.F., Pritchard, J.A., 1978. Satellite detection of urban heat islands. Mon. Weather Rev. 106, 1725–1734.

Myint, S.W., Gober, P., Brazel, A., Grossman-Clarke, S., Weng, Q., 2011. Per-pixel vs. object-based classification of urban land cover extraction using high spatial resolution imagery. Remote Sens. Environ. 115, 1145–1161.

Oke, T.R., 1976. The distinction between canopy and boundary-layer heat islands. Atmosphere 14, 268–277.

Owen, T.W., Carlson, T.N., Gillies, R.R., 1998. An assessment of satellite remotely-sensed land cover parameters in quantitatively describing the climatic effect of urbanization. Int. J. Remote Sens. 19, 1663–1681.

Palme, M., Lobato, A., Carrasco, C., 2016. Quantitative analysis of factors contributing to urban heat island effect in cities of latin-American Pacific coast. Procedia Eng. 169, 199–206.

Paulinaa, W., Poh-Chin, L., Melissab, H., 2015. Temporal statistical analysis of urban heat islands at the microclimate level. Procedia Environ. Sci. 26, 91–94.

Peres, L.F., Libonati, R., DaCamara, C.C., 2014. Land-Surface emissivity retrieval in MSG–SEVIRI TIR channels using MODIS data. IEEE Trans. Geosci. Remote Ses. 52, 5587–5600.

Pinheiro, A.C.T., Hook, S., Prigent, C., Knuteson, R., Bosilovich, M., Rossow, W., Viterbo, P., 2008. International Workshop on the Retrieval and Use of Land Surface Temperature: Bridging the Gaps – Summary Report. National Climatic Data Center Asheville, NC, pp. 1–39 April 7–9, 2008.

Qin, Z., Kamieli, A., Berliner, P., 2001. A mono-window algorithm for retrieving land surface temperature from Landsat TM data and its application to the Israel-Egypt border region. Int. J. Remote Sens. 22, 3719–3746.

Rao, P.K., 1972. Remote sensing of urban heat islands from an environmental satellite. Bull. Am. Meteorol. Soc. 53, 647–648.

Rhinane, H., Hilali, A., Bahi, H., Berrada, A., 2012. Contribution of Landsat tm data for the detection of urban heat islands areas case of Casablanca. J. Geogr. Inf. Syst. 4, 20–26.

Roth, M., 2007. Review of urban climate research in (sub) tropical regions. Int. J. Climatol. 27, 1859–1873.

Roy, R.P., Wulder, M.A., Loveland, T.R., et al., 2014. Landsat-8: science and product vision for terrestrial global change research. Remote Sens. Environ. 145, 154–172.

Schroeder, W., Csiszar, I., Morisette, J., 2008. Quantifying the impact of cloud obscuration on remote sensing of active fires in the Brazilian Amazon. Remote Sens. Environ. 112, 456–470.

Sobrino, J.A., Oltra-Carrió, R., Jiménez-Muñoz, J.C., Julien, Y., Sòria, G., Franch, B., Matta, C., 2012. Emissivity mapping over urban areas using a classification-based approach: application to the Dual-use European Security IR Experiment (DESIREX). Int. J. Appl. Earth Obs. Geoinf. 18, 141–147.

Souza, J.D., Silva, B.B., 2005. Correção atmosférica para temperatura da superfície obtida com imagem TM: Landsat 5. Revista Brasileira de Geofísica 23, 349–358.

Taha, H., 1997. Urban climates and heat islands: albedo, evapotranspiration, and anthropogenic heat. Energy Build. 25, 99–103.

Trenberth, K.E., Jones, P.D., Ambenje, P., Bojariu, R., Easterling, D., Klein Tank, A., Parker, D., Rahimzadeh, F., Renwick, J.A., Rusticucci, M., Soden, B., Zhai, P., 2007. In: Solomon, S., Qin, D., Manning, M., Chen, Z., Marquis, M., Averyt, K.B., Tignor, M., Miller, H.L. (Eds.), Climate Change 2007: The Physical Science Basis. Contribution of Working Group I to the Fourth Assessment Report of the Intergovernmental Panel on Climate Change. Cambridge University Press Cambridge, United Kingdom and New York, NY, USA.

United Nations, 2014. Department of Economic and Social Affairs, Population Division, . World Urbanization Prospects: The 2014 Revision, Highlights. (ST/ESA/SER.A/352).

Van de Griend, A.A., Owe, M., 1993. On the relationship between thermal emissivity and the normalized difference vegetation index for natural surfaces. Int. J. Remote Sens. 14, 1119–1131.

Vlassova, L., Perez-Cabello, F., Nieto, H., Martín, P., Riaño, D., de la Riva, J., 2014.

Assessment of methods for land surface temperature retrieval from Landsat-5 TM images applicable to multiscale tree-grass ecosystem modeling. Remote Sens. 6, 4345.

Voogt, J.A., Oke, T.R., 2003. Thermal remote sensing of urban climates. Remote Sens. Environ. 86, 370–384.

Wanga, Y., Berardib, U., Akbaria, H., 2015. The urban heat island effect in the city of Toronto. Procedia Eng. 118, 137–144.

Weng, Q.E., Quattrochi, D.A., 2006. Thermal remote sensing of urban areas: an introduction to the special issue. Remote Sens. Environ. 104, 119–122.

Wilks, D.S., 2006. Statistical Methods in the Atmospheric Sciences, 2 ed. Academic Press, London.

Windahl, E., de Beurs, K., 2016. An intercomparison of Landsat land surface temperature retrieval methods under variable atmospheric conditions using in situ skin temperature. Int. J. Appl. Earth Obs. Geoinf. 51, 11–27.

Zhou, J., Li, J., Zhang, L.X., Hu, D.Y., Zhan, W.F., 2012. Intercomparison of methods for estimating land surface temperature from a Landsat-5 TM image in an arid region with low water vapour in the atmosphere. Int. J. Remote Sens. 33, 2582–2602.